Generalisation of the eddy-dissipation concept for jet flames with low turbulence and low Damköhler number

M.J. Evans[a,*], C. Petre[b], P.R. Medwell[a], A. Parente[c]

[a]*School of Mechanical Engineering, The University of Adelaide, South Australia, 5005, Australia*
[b]*ANSYS Belgium, Avenue Pasteur, 4, 1300 Wavre, Belgium*
[c]*Ecole Polytechnique de Bruxelles, Aero-Thermo-Mechanics Laboratory, Université Libre de Bruxelles, Brussels, 1050, Belgium*

Abstract

Moderate or intense low oxygen dilution (MILD) combustion has been the focus of a range of fundamental experimental and numerical studies. Reasonable agreement between experimental and numerical investigations, however, requires finite-rate chemistry models and, often, *ad hoc* model adjustment. To remedy this, an adaptive eddy dissipation concept (EDC) combustion model has previously been developed to target conditions encountered in MILD combustion; however, this model relies on a simplified, pre-defined assumption about the combustion chemistry. The present paper reports a generalised version of the modified EDC model without the need for an assumed, single-step chemical reaction or *ad hoc* coefficient tuning. The results show good agreement with experimental measurements of two CH_4/H_2 flames in hot coflows, showing improvements over the standard EDC model as well as the previously published modified EDC model. The updated version of

*Corresponding author. E-mail: m.evans@adelaide.edu.au, Tel.: +61 8 8313 5460, Fax: +61 8 8313 4367.

May 11, 2018

the EDC model also demonstrates the capacity to reproduce the downstream transition in flame structure of a MILD jet flame seen experimentally, but which has previously proven challenging to capture computationally. Analyses of the previously identified dominant heat-release reactions provide insight into the structural differences between a conventional autoignitive flame and a flame in the MILD combustion regime, whilst highlighting the requirement for a generalised EDC combustion model.

Keywords: Eddy Dissipation Concept, MILD Combustion, Vitiated Coflow

1. Introduction

Combustion in the moderate or intense low oxygen dilution (MILD) regime has been identified as offering improved efficiency and reduced pollutant emissions [1]. To better understand non-premixed MILD combustion, fundamental research has been undertaken using jet-in-hot-co-/cross-flow (JHC) burners [2, 3] which emulate practical combustion systems utilising sequential combustion or exhaust gas recirculation (EGR). Despite extensive investigations, these experimental studies have proved challenging to model, due to the relatively slow chemical time-scales and low turbulence intensity. Under these conditions, local chemical and turbulence time-scales are similar and diffusivity has a significant impact on flame stabilisation [4]. Additionally, direct numerical simulations (DNS) have revealed interacting reaction zones which may locally favour autoignition or propagation under MILD combustion conditions [5]. These features invalidate common combustion model assumptions of: infinitely fast-chemistry, that reaction-zones may be described as an ensemble of strained opposed-flames, or that well-mixed chemical species react at the finest scales of turbulence [6, 7].

A characteristic feature of MILD combustion in JHC burners is strong turbulence-chemistry interactions, resulting in a Damköhler number, Da, near unity [7]. As a result, computational modelling of MILD jet flames requires a finite-rate chemistry approach, with the eddy dissipation concept (EDC) model [8] previously demonstrating reasonable accuracy and computational cost [4, 6, 7, 9, 10]. The EDC model uses the assumption that a reacting flow-field may be discretised into a network of perfectly-stirred reactors within "fine structures" at the Kolmogorov length-scale [8]. The

reaction rate of any given species in each reactor is derived from theoretical arguments, based on the semi-empirical turbulent energy cascade between length-scales [8]. Furthermore, by transporting individual mass fractions, the EDC may be used in arbitrary flows, without a pre-defined mixture fraction, in contrast to flamelet models [11].

It has been shown that the standard EDC model cannot be applied in flames where values of the turbulence Reynolds number, Re_T, are low [6, 7, 9]. Under such conditions, the EDC model has required *ad hoc* adjustments of the empirically-derived model coefficients to fit experimental measurements and avoid artificially limiting reaction-zone length-scales [6, 9, 10]. The previously identified deficiencies of the EDC model at low Re_T has prompted the extension of the EDC, with dynamic coefficients derived in terms of Re_T and Da [7]. This modified model introduced empirical blending coefficients between the low Re_T form and the standard EDC model, however, required a global estimate of reaction rates to estimate Da [7]. Such an approach for adaptive EDC length-scale calculations, based on both turbulence and chemistry, has also been suggested during the analyses of DNS studies [5]. Physical interpretation of the adjusted EDC coefficients used with Reynolds-averaged Navier-Stokes (RANS) flow-fields can indicate the reaction zone time- and length-scales throughout a flame, and describe distinguishing features of MILD combustion. Previous work has suggested that, under MILD combustion conditions in a JHC burner, reaction zones are smaller than in conventional combustion [6, 7, 9] with longer residence times [6, 7, 9], reducing local reaction rates [4, 6–10].

This work presents a revised version of the modified EDC model proposed

by Parente *et al.* [7], incorporating detailed chemical kinetics to evaluate Da, to better estimate chemical time-scales and reaction rates. Following comparisons against previous experimental measurements [2], the structure of the flames are analysed, and contrasted, in terms of reaction-zone scales and regions of heat release.

2. Model Description

2.1. The Modified Eddy Dissipation Concept

The eddy dissipation concept (EDC) combustion model is a multi-species, finite-rate combustion model. The key assumption in the derivation of the EDC model is that all reactions are confined to "fine structures" [8]. These reactions are governed by a reaction rate derived on the assumption that all energy is transferred to, and dissipated at, the smallest length-scales [8]. There is, however, evidence to suggest that there may be energy transfer to larger scales in [premixed] reacting flows for Da on the order of unity [12]. This is consistent with the interacting reaction zones in MILD combustion revealed by DNS [5]. The characteristic mass fraction, γ, and time, τ^*, of fine scales may be given as multiples of the Kolmogorov length- and time-scales [7, 8]:

$$\gamma = C_\gamma(\nu\varepsilon/k^2)^{1/4} \tag{1}$$

$$\tau^* = C_\tau(\nu/\varepsilon)^{1/2}, \tag{2}$$

leading to the reaction rate of species i, R_i [7]:

$$R_i = \rho\gamma^2/[\tau^*(1-\gamma^3)](Y_i - Y_i^*) \tag{3}$$

where ρ is the mean density, ν the kinematic viscosity, ε the dissipation rate, k the turbulent kinetic energy and Y_i and Y_i^* are the mass fractions of species i surrounding, and within, the scales, respectively. The coefficients C_τ and C_γ are empirically derived and held constant for all scenarios in the original EDC model [8].

Theoretical derivation of the modified EDC combustion has been previously provided by Parente *et al.* [7] and is not reproduced here. This reformulates the EDC model coefficients as functions of $Re_T = k^2/(\varepsilon\nu)$ and Da evaluated at the Kolmogorov length-scale. Based on the energy cascade assumed in the k-ε turbulence model, the modified EDC [7, 13] introduces a relationship for the coefficients, such that:

$$C_\tau = 1/2[Da_\eta^2(Re_T + 1)]^{-1/2} \tag{4}$$

$$C_\gamma = (2/3)^{1/2}[Da_\eta(Re_T + 1)]^{1/2}. \tag{5}$$

The coefficient in Eq. (4) was derived analytically [13], however, the coefficient in Eq. (5) differs from the value proposed in alternate form for C_γ [13]. The alternate form estimates the fine-structures size, L^*, as the product of the chemical time-scale, τ_c, and laminar flame-speed, S_L ($L^* = \tau_c S_L$) [13]. Conversely, the derivation leading to Eq. (4), assumes $L^* \propto \tau_c S_L$ [7]. Additional dependency on fluid properties, such as thermal diffusivity, is hypothesised and under further investigation.

Equations (4) and (5) are used for $Re_T > 5$, and $\tau_c, < 0.1$ s which, in-turn, are obtained from the modelled flow-field and detailed chemical kinetics. Outside of these ranges, the values of C_τ and C_γ are set to those proposed

by Magnussen [8]. Results were found to be insensitive to changes in these cut-off values by up to an order of magnitude. Finally, the coefficients are bound by those originally derived by Magnussen for a fully turbulent flow [8] and the values differing by an order of magnitude: C_τ is limited between 0.4083 [8] and 5.0, and C_γ to between 0.5 and 2.1377 [8]. Values of C_τ and C_γ which are respectively below and above the values estimated by Magnussen [8] tend towards infinitely fast chemistry, which is unsuitable for modelling flames with Da near unity. Although values of C_τ below 0.4083 have been suggested for MILD combustion [14], reducing the limit of C_τ to 0.05 did not affect the results.

Local values of Da_η have previously been estimated using a global reaction rate [15] for one-step CH_4 combustion [7]. This estimation is fuel-specific and cannot account for finite-rate reactions, which are controlled by minor species in different regions of the flame. There is hence a need to extend this to a general form without explicit dependency on the boundary conditions. In this work, Da_η is calculated as the ratio of the flow time-scale, τ_f, to τ_c:

$$\tau_f = (\nu/\varepsilon)^{1/2} \tag{6}$$

$$\tau_c = \max[Y_i/(|\omega_i|/\rho)]. \tag{7}$$

Here, ω_i are the reaction rates (in kg/m^3/s) of CH_4, H_2, O_2, CO and CO_2, as these slower major species dominate the fine-scale time-scales and larger flame structure [16]. Small $\omega_i < 10^{-16}$ kg/m^3/s, and hence large τ_c, were ignored to exclude local non-reacting species, such that τ_c is the local limiting chemical time-scale. This method of estimating τ_c is significantly faster than

methods derived from calculating eigenvalues of the Jacobian, and could also readily be implemented with the previously mentioned alternate form of C_γ for an improved estimate of Da [13]. Finally, a characteristic Reynolds number for fine scales, Re^*, was defined such that $Re^* = 1$ at the Kolmogorov length-scale and 2.5 for the standard EDC model [7], where:

$$Re^* = 4/3 C_\tau C_\gamma^2. \tag{8}$$

Although the HM1 and HM3 test cases [2] are studied closely for MILD combustion, these are only examples of low Re_T flames which have previously required *ad hoc* coefficient tuning [6, 7, 9]. The revised form of the EDC model recovers the constants of the standard EDC model ($C_\tau = 0.4083$ and $C_\gamma = 2.1377$) for $Re_T > 500$, which have been validated against data collected from highly turbulent flames [17].

2.2. Calculation of Mixture Fraction

The stoichiometric reactants of a hydrocarbon fuel may be written as $a_i \mathrm{C}_{m_i}\mathrm{H}_{n_i}\mathrm{O}_{p_i} + \nu \mathrm{O}_2$, where $\sum_{i=1}^{N} a_i = 1$. Denoting the fuel and oxidiser streams as F and Ox respectively, atomic mixture fraction, Z_i, and atomic weight, W_i, the mixture fraction relating a single fuel stream to a single oxidant stream may be written as [18]:

$$Z = \frac{\frac{Z_C - Z_{C,Ox}}{a_i m_i W_C} + \frac{Z_H - Z_{H,Ox}}{a_i n_i W_H} - \frac{Z_O - Z_{O,Ox}}{\nu W_O}}{\frac{Z_{C,F} - Z_{C,Ox}}{a_i m_i W_C} + \frac{Z_{H,F} - Z_{H,Ox}}{a_i n_i W_H} - \frac{Z_{O,F} - Z_{O,Ox}}{\nu W_O}}. \tag{9}$$

Extending this description of mixture fraction to the "three stream" configuration needed for flames stabilised on JHC burners [19], requires two independent mixture fractions: Z_1 is defined as the mixture fraction between the fuel and the hot coflow and Z_2 is the mixture fraction between the fuel

and the wind tunnel air stream. Assuming that diffusive mixing between the two oxidants is dominated by N_2, $Le = 1$, a weighting factor, S_N, can be defined as:

$$S_N = \frac{Z_{N,2} - Z_{N,F} - Z_N}{Z_{N,2} - Z_{N,F} - Z_{N,1}} \tag{10}$$

where Z_N is the mass fraction of element N. This results in a global mixture fraction, Z_W:

$$Z_W = S_N Z_1 + (1 - S_N) Z_2. \tag{11}$$

The distributions of Z_W and S_N may be used to gauge the influence of the oxidant streams, and their mixing, on the flame structure.

3. Numerical Setup

Previously studied CH_4/H_2 flames [2] are computed using a modified EDC model [7] in ANSYS FLUENT 17.2. Both these flames have a bulk mean jet Reynolds number of 10,000 and have been previously investigated numerically [4, 6, 7, 14, 20].

The domain for the 1:1 CH_4/H_2 (by volume) flames [2] has been used previously for the same cases with a modified EDC model [7], and was mesh independent. This study focuses on two flames issuing into 1300-K coflows with 3 or 9% O_2 (by mass), referred to as HM1 and HM3 [2], with $Z_{st} = 0.007$ and $Z_{st} = 0.021$, respectively. This study uses the generalised EDC model described in §2.1 for turbulence-chemistry interactions and the five-equation Reynolds stress model (RSM), with a quadratic pressure-strain relationship, for modelling the underlying flow-field. All other aspects of the simulations are the same as those used previously by Parente *et al.* [7] for direct comparison. This includes the use of the KEE-58 mechanism, with 16 species and 58

reactions [21]. For additional validation, temperature profiles are compared to more detailed kinetics mechanisms in the Supplementary Data.

It should be noted that, when starting from a partially converged reacting flow-field, the use of the use of the revised EDC model does not require a significant increase in computational time compared to the standard EDC model and similar convergence can be achieved. The revised EDC model also benefits from *in-situ* adaptive tabulation for reducing solution times [22].

4. Results and Discussion

4.1. Verification of Generalised EDC Model

Radial profiles of temperature, Y_{CO}, Y_{OH} and Y_{H_2O} for the HM1 and HM3 flames are presented in Figs. 1 and 2. These figures show comparisons of the current, and previous modelling efforts (labelled "Fuel 2016") [7], along with experimental data [2]. The form of Eq. (5) proposed by Bao [13], gave similar results from the standard EDC model [8]. Estimated 95% confidence intervals [7] of the experimental means [2] were similar to the span of the glyphs used for the data. The differences between the peak temperature values obtained through CFD and those measured experimentally are tabulated in the Supplementary Data.

Comparison of the newly predicted values show better agreement than the other EDC models in the majority of plots in Figs. 1 and 2. Examination of Fig. 1 demonstrates the superior predictive qualities of the revised EDC model compared to the standard EDC and the previous, modified EDC model [7]. These results demonstrate excellent prediction of temperature and the peak concentrations of OH and H_2O throughout the flame, as well as the

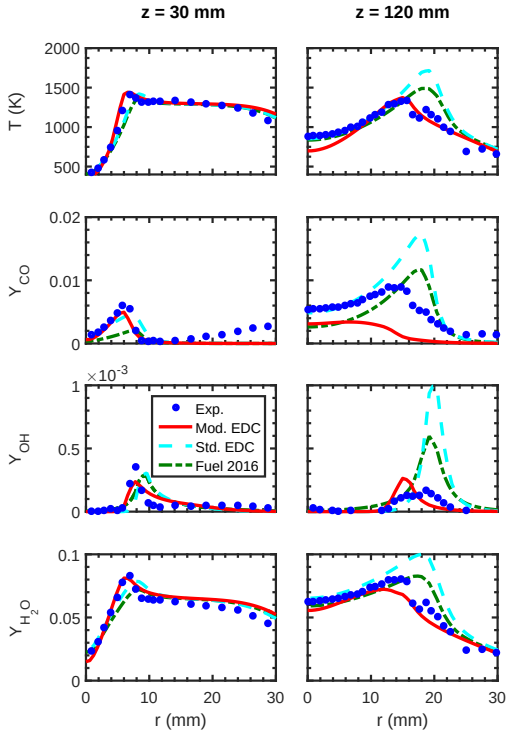

Fig. 1: Comparisons of experimental [2] and predicted radial temperature, Y_{CO}, Y_{OH} and $Y_{\mathrm{H_2O}}$ distributions for the HM1 flame at two downstream locations. The current modelling is referred to as "Mod. EDC", the standard EDC model [8] is referred to as "Std. EDC" and the work of Parente *et al.* [7] is referred to as "Fuel 2016".

concentration of CO in the near-field, 30 mm from the jet exit plane. The current EDC model demonstrates the best predictions of the magnitude and locations of peak temperature in the HM1 case. Similarly, the new approach gives improved predictions of near-field CO and H_2O, with similar predictions of OH to the two other models. Results at 60 mm from the jet exit plane (omitted for brevity) showed similar predictive qualities to results taken at 30 mm. These results indicate a significant improvement in modelling the major features of the MILD HM1 flame [2]. Although similar accuracy in modelling this flame has been achieved using RANS approaches [6, 7, 14],

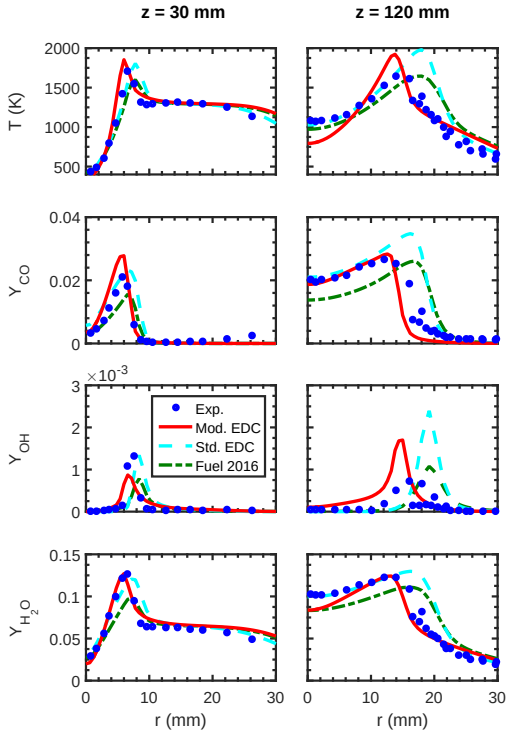

Fig. 2: Comparisons of experimental [2] and predicted radial temperature, Y_{CO}, Y_{OH} and $Y_{\mathrm{H_2O}}$ distributions for the HM3 flame at two downstream locations. The current modelling is referred to as "Mod. EDC", the standard EDC model [8] is referred to as "Std. EDC" and the work of Parente *et al.* [7] is referred to as "Fuel 2016".

these results were obtained with either coefficient tuning [6, 14] or a pre-set reaction time-scale [7]. Similarly, the current model shows an improved prediction of temperature in the HM3 case at 30 mm, with only a slight under-prediction of OH concentration (Fig. 2). In both cases, the features of the flame are well predicted in the coflow-dominated region of the flame ($\lesssim$ 100 mm from the jet exit [2]).

Beyond the coflow-controlled region, the results in both Fig. 1 and 2 show improved predictions of temperature, OH and H_2O mass fractions compared to the standard EDC model and the previous study by Parente *et al.* [7]. Of

the different EDC models, only the current approach is able to predict the decrease in peak temperature in the HM1 flame at the downstream location (see Fig. 1). Although the current model slightly over-predicts both temperature and OH concentration in the HM3 case at the same location, it offers an improvement over the standard EDC without the *ad hoc* modification of coefficients or any prior estimates about chemical time-scale. The distribution and peak mass fraction of CO at 120 mm from the jet exit plane are both captured in the HM3 flame, however, the magnitude is under-predicted in the HM1 case. This, however, is consistent with the discrepancies seen in the initial one-dimensional opposed-flame calculations [2], which was attributed to improper treatment of low-temperature CO pathways in reduced chemical kinetics of CH_4 oxidation [2, 14], such as the one used in this study. These results are a step towards validating the revised EDC model for use in low Re_T and low Da jet flames.

The revised EDC demonstrates the best agreement in temperature across the two flames over both measurement locations. Values of Re_T (not shown for brevity) in the shear layer range from 2-50 for both flames, significantly less than the valid range of the standard EDC model [9]. This increases to $Re_T \sim 300$ along the jet centreline, as well as in the hot coflow region—indicating both the low turbulence level of the jet and the laminarising effects of the hot coflow. This demonstrates the effectiveness of the revised EDC combustion model in predicting the structure of the HM1 flame HM3 flames, which may be described as MILD and autoignitive respectively near the jet exit plane [23].

4.2. Global Flame Features

Distributions of the three-stream weighting factor, S_N, in Fig. 3 demonstrate the mixing of the cold, wind tunnel air stream. Values of $S_N = 1$ and 0 are used to distinguish between the hot coflow and wind tunnel air, respectively. Negative values of S_N are indicative of mixing with the (pure hydrocarbon) fuel stream. This figure, and Fig. 4, are replicated for the "Std. EDC" and "Fuel 2016" [7] cases as Supplementary Data.

Figure 3 demonstrates that the coflow stream controls the oxidant composition for approximately 150 mm downstream of the jet exit plane, after which the entrained air controls the local oxidant composition. This region of high dilution corresponds with the broad, high-temperature region of the HM1 flame shown in Fig. 4, which initiates approximately 170 mm from the jet exit plane. This broadened high temperature region corresponds to higher values of S_N, indicating an increased availability of O_2 from air entrainment. Air entrainment into the fuel jet stream is enhanced in the HM1 case, as a result of reaction zone weakening [24], resulting in a more sudden temperature increase in the HM1 case than in the HM3 flame. This sudden increase in temperature may initially appear to suggest an autoignitive, lifted flame base, however, the HM1 flame is attached. The HM1 flame demonstrates a gradual increase in temperature with downstream distance from the jet exit plane, consistent with previous descriptions of non-premixed flame stabilisation in the MILD combustion regime [23], unlike conventional autoginitive flames [25]. These results are in contrast to previous EDC modelling studies which significantly over-predict the mean near-field temperature in the HM1 flame [4, 20], exhibiting a smooth increase in temperature along the entire

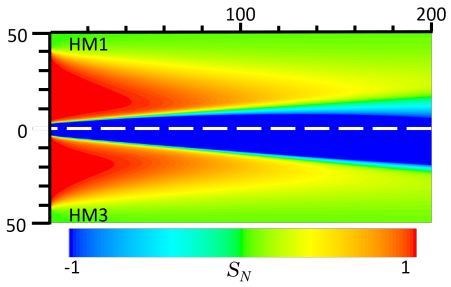

Fig. 3: Three-stream weighting factor, S_N for the HM1 and HM3 flames, images extend 50 mm radially, and 200 mm downstream of the jet exit plane.

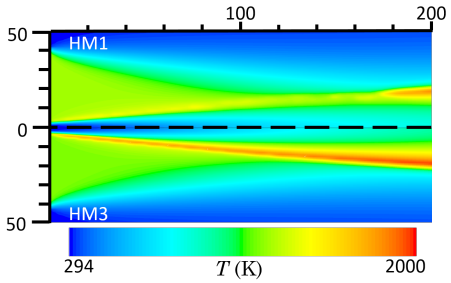

Fig. 4: Temperature field for the HM1 and HM3 flames, images extend 50 mm radially, and 200 mm downstream of the jet exit plane.

length of the flame [20]. As a consequence, these modelling studies [4, 20] could not reproduce the change in flame structure observed experimentally with air entrainment [2].

Spatial distributions of Da_η, the EDC model variables, C_τ and C_γ, and Re^*, may be used to complement the mixture fraction and temperature fields and provide further insight into the structure of the HM1 and HM3 flames. These are presented in Figs. 5-8 respectively. Additionally, distributions of Re_T are included as Supplemental Data. The distribution of Da_η in the HM1 flame (Fig. 5) shows a distinct transition from a weak, thin reaction zone to a more intensely burning region with a change from $Da_\eta < 0.1$ to

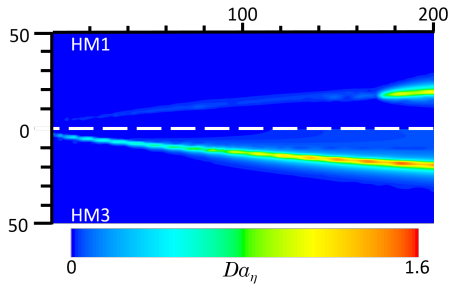

Fig. 5: Damköhler number for the HM1 and HM3 flames, images extend 50 mm radially, and 200 mm downstream of the jet exit plane.

$Da_\eta > 0.1$. This transition point is also evident in the temperature (Fig. 4) and OH (not shown for brevity) distributions, which can both be measured experimentally. Although this transition is similar in appearance to the transitional structure seen in ethylene [3, 6] flames, the transition in the HM1 flame occurs approximately 170 mm downstream, and hence is likely to be the effect of air entrainment from the surrounding wind tunnel rather than a two-stage ignition process in the coflow-controlled region [26]. In contrast to the sudden change in the Da_η profile of the HM1 flame, the distribution of Da_η in the HM3 flame suggests an attached flame without a noticeable discontinuity across the transition from the coflow-controlled near-field to the air-dominated downstream flame brush.

The distributions of C_τ and C_γ in Figs. 6 and 7 highlight the requirement for the current adaptive EDC model. These figures show that both C_τ and C_γ vary significantly within both flames, contradicting the assertion that they are constant across all turbulent flows [8]. The results indicate that the greatest change in the modified coefficients, relative to the standard model values, occur at the transition point of the HM1 flame and near the jet centreline in the stabilisation region of the HM3 flame. In these regions,

C_τ is increased whilst C_γ is reduced, analogous to an increase in the residence times of the modelled perfectly-stirred reactors in the EDC model, with a simultaneous reduction in the reacting mass fractions within the fine the structures, quantified in Eqs. (4) and (5). The same trend was observed in a study of ethylene jet flames in hot and diluted coflows, following manual tuning of the standard EDC model parameters [6]. This was interpreted as an indication of stretched fine structures with increased residence times, containing less energetic fluid, owing to the reduced O_2 concentration associated with MILD combustion [6]. Similarly, the low Re_T of the shear layer in these cases has a negative impact on mixing which increases residence times and reduces the reactivity of the fine structures.

The changes in C_τ and C_γ result in the increased Re^* upstream of the HM1 transition point, and on the rich side of both flames. In these locations, local values of Re^* are several times larger than in the standard EDC model. Interestingly, regions of low Re^* near the centreline of the HM3 flame are not seen in the HM1 case. In contrast, the HM1 case exhibits high values of Re^*, C_τ and low C_γ near the shear layer of the MILD HM1 flame, which are not seen in the HM3 flame. This indicates that the flame structure of the current model deviates most significantly from the standard EDC model near the shear layer of the HM1 flame. Notably, in this region, Re^* takes similar values to those predicted using global constants in this configuration [7]. However, unlike implementations using global constants [7], the new model recovers the expected $Re^* = 2.5$ away from the jet. These results identify key differences between the reaction zone structures in the two flames, and the inability of the standard EDC model to predict them.

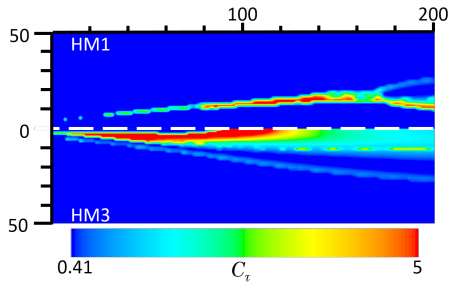

Fig. 6: Modelled values of C_τ for the HM1 and HM3 flames, images extend 50 mm radially, and 200 mm downstream of the jet exit plane.

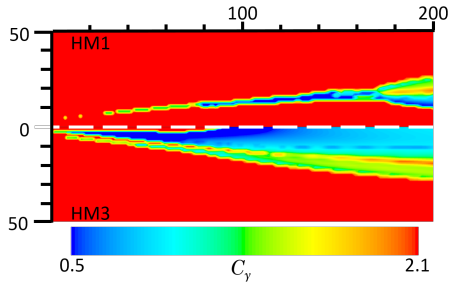

Fig. 7: Modelled values of C_γ for the HM1 and HM3 flames, images extend 50 mm radially, and 200 mm downstream of the jet exit plane.

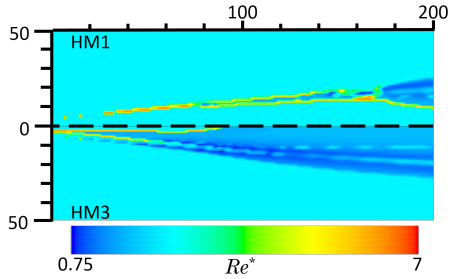

Fig. 8: Modelled characteristic fine structure Reynolds number for the HM1 and HM3 flames, images extend 50 mm radially, and 200 mm downstream of the jet exit plane.

4.3. Local Distributions of Radical Species

The characteristic reaction rate parameters shown in Figs. 5-8 correspond to changes in the time-averaged reaction zone structure of the HM1 and HM3

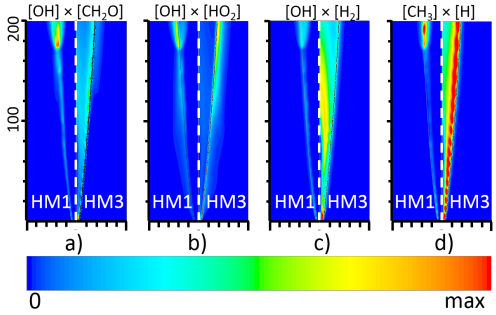

Fig. 9: Reactants of the dominant exothermic reactions for the HM1 and HM3 flames, each image shows 50 mm in the radial direction and extends 200 mm downstream of the jet exit plane.

flames. These parameters are strongly coupled to the underlying chemical and flow-fields and, hence, the local heat-release rate. Figures 9a)-d) show the fields of relative $[OH]\times[CH_2O]$, $[OH]\times[HO_2]$, $[OH]\times[H_2]$ and $[CH_3]\times[H]$. Ranges of each distribution are identical for the HM1 and HM3 comparisons, but are different for each pair of images. They are additionally superimposed with the $Z_1 = Z_{1,st}$ contour. The species pairs in Figs. 9a)-d) are the reactants of the major exothermic reactions in the HM1-3 flames [27]. As such, the product of their concentrations may be considered as heat-release markers in different parts of the flames [27]. All of these measures suggest a region of strong heat-release near the jet exit of the HM3 flame which is not seen in the less-intense, more-uniform HM1 case.

In the HM1 and HM3 flames, the heat-release indicator of $[OH]\times[HO_2]$ initially extends from the flame front into the hot coflow region (see Fig. 9a)). In contrast, the distributions of $[OH]\times[CH_2O]$, $[OH]\times[H_2]$ and $[CH_3]\times[H]$ extend from stoichiometric to rich mixtures in the HM3 case, but follow $Z_{1,st}$ in the HM1 case. Significantly, $[OH]\times[HO_2]$ in the rich side of the HM3 reac-

tion zone demonstrates the presence of HO_2 near the jet exit plane (Fig. 9b)). A similar distribution occurs further downstream in the HM1 case, and has previously been used to indicate tribrachial flame bases in planar, coflowing laminar flames with the same composition [27]. The concentration of HO_2 (not shown for brevity) in the HM3 case slowly diminishes with downstream distance, albeit in regions of higher diffusivity, suggesting that the HO_2 originates from a build-up at the flame base, as seen in laminar flames [27]. The overlap of $[OH]\times[CH_2O]$, $[OH]\times[H_2]$ and $[CH_3]\times[H]$ are very different between the HM1 and HM3 flames. Heat release indicated by $[CH_3]\times[H]$ is the most exothermic reaction involving CH_3 in the HM1 and HM3 flames [27] and, unlike $[OH]\times[CH_2O]$, $[OH]\times[H_2]$ is not dependent on O/OH diffusion across the reaction zone. The $[CH_3]\times[H]$ marker is prevalent near the centreline of the HM3 flame, although neither species is present in significant quantities in the coflow-controlled region of the HM1 flame (omitted for brevity). In the HM3 case, these species are formed near the jet centreline and, in-turn, react exothermically to promote further fuel decomposition to sustain the supply of radicals to the flame front. The absence of any regions of significant rich or lean indicating HM1 case suggests that the heat-release near the jet exit plane is insufficient to initiate the thermal decomposition of either CH_4 or H_2 in the jet through preheating. This serves to explain the significantly weaker flame-front, lower local Da_η and, hence, the differences in C_τ and C_γ between the two flames.

5. Conclusions

A revised EDC model for low Re_T and low Da combustion has been presented without the need for *ad hoc* coefficient tuning or estimations of

a representative, one-step chemical reaction. The results from this model show very good agreement with previously measured temperature and species concentration data in the low turbulence intensity region near the jet exit plane of the HM1 and HM3 flames [2]. Further downstream, the model captures the increase in Da_η corresponding to the HM1 flame brush seen experimentally [2] and indicates changes in characteristic Re^* which cannot be predicted by the standard EDC model. The results show the build-up of radical species and ignition precursors along the centreline of the HM3 flame. Conversely, in the MILD HM1 case, stabilisation is sustained only by reactions near the jet shear layer. The two significantly different structures demonstrate the range of Da and Re_T encountered in simple turbulent flames, and the adaptability of the generalised EDC combustion model.

Acknowledgements

M. J. Evans and P. R. Medwell acknowledge support from the University of Adelaide, the Australian Research Council (ARC) through the Discovery (DP and DECRA) grant scheme, the United States Asian Office for Aerospace Research and Development (AOARD), and eResearch SA for high-performance computing.

References

[1] A. Cavaliere, M. de Joannon, Prog. Energ. Combust. 30 (2004) 329–366.

[2] B. Dally, A. Karpetis, R. Barlow, Proc. Combust. Inst. 29 (2002) 1147–1154.

[3] P. R. Medwell, P. A. M. Kalt, B. B. Dally, Combust. Flame 152 (2008) 100–113.

[4] F. C. Christo, B. B. Dally, Combust. Flame 142 (2005) 117–129.

[5] Y. Minamoto, N. Swaminathan, S. R. Cant, T. Leung, Combust. Flame 161 (2014) 2801–2814.

[6] M. J. Evans, P. R. Medwell, Z. F. Tian, Combust. Sci. Technol. 187 (2015) 1093–1109.

[7] A. Parente, M. R. Malik, F. Contino, A. Cuoci, B. B. Dally, Fuel 163 (2016) 98–111.

[8] B. F. Magnussen, in: ECCOMAS thematic conference on computational combustion, Lisbon, Portugal. June 21–24, 2005.

[9] A. De, E. Oldenhof, P. Sathiah, D. Roekaerts, Flow Turbul. Combust. 87 (2011) 537–567.

[10] S. R. Shabanian, P. R. Medwell, M. Rahimi, A. Frassoldati, A. Cuoci, Appl. Therm. Eng. 52 (2013) 538–554.

[11] E. Abtahizadeh, P. de Goey, J. van Oijen, Combust. Flame 162 (2015) 4358–4369.

[12] J. O'Brien, C. A. Towery, P. E. Hamlington, M. Ihme, A. Y. Poludnenko, J. Urzay, Proc. Combust. Inst. 36 (2017) 1967–1975.

[13] H. Bao, Development and Validation of a New Eddy Dissipation Concept (EDC) Model for MILD Combustion, Master's thesis, TU DELFT, 2017.

[14] A. Mardani, Fuel 191 (2017) 114–129.

[15] C. K. Westbrook, F. L. Dryer, Prog. Energy Combust. Sci. 10 (1984) 1–57.

[16] B. J. Isaac, A. Parente, C. Galletti, J. N. Thornock, P. J. Smith, L. Tognotti, Energy Fuels 27 (2013) 2255–2265.

[17] D. A. Lysenko, I. S. Ertesvåg, K. E. Rian, Flow, Turbul. Combust. 93 (2014) 577–605.

[18] N. Peters, Turbulent Combustion, Cambridge University Press, 2000.

[19] M. Ihme, Y. C. See, Proc. Combust. Inst. 33 (2011) 1309–1217.

[20] J. Aminian, C. Galletti, L. Tognotti, Fuel 165 (2016) 123–133.

[21] R. Bilger, S. Stårner, R. Kee, Combust. Flame 80 (1990) 135–149.

[22] S. Pope, Combust. Theor. Model. 1 (1997) 41–63.

[23] M. J. Evans, P. R. Medwell, H. Wu, A. Stagni, M. Ihme, Proc. Combust. Inst. 36 (2016) 4297–4304.

[24] P. R. Medwell, P. A. M. Kalt, B. B. Dally, Combust. Sci. Technol. 181 (2009) 937–953.

[25] C. S. Yoo, E. S. Richardson, R. Sankaran, J. H. Chen, Proc. Combust. Inst. 33 (2011) 1619–1627.

[26] P. R. Medwell, M. J. Evans, Q. N. Chan, V. R. Katta, Energy Fuels 30 (2016) 8680–8690.

[27] M. J. Evans, P. R. Medwell, Z. F. Tian, J. Ye, A. Frassoldati, A. Cuoci, Combust. Flame 178 (2017) 297–310.

List of Figures